Chemical Engineering Science 80 (2012) 334–341

Contents lists available at SciVerse ScienceDirect

Chemical Engineering Science

journal homepage: www.elsevier.com/locate/ces

Mixing patterns in water plugs during water/ionic liquid segmented flow in microchannels

Valentina Dore, Dimitrios Tsaoulidis, Panagiota Angeli *

Department of Chemical Engineering, University College London, Torrington Place, WC1E 7JE London, UK

HIGHLIGHTS

- Plug flow in microchannels using ionic liquid.
- Image analysis to obtain PIV velocity maps and plug characteristics.
- Secondary vortices found in plugs at medium mixture velocities.
- New correlation for film thickness.
- Circulation time profiles depend on mixing velocity and plug length.

ARTICLE INFO

Article history:
Received 12 April 2012
Received in revised form
14 June 2012
Accepted 15 June 2012
Available online 23 June 2012

Keywords:
Multiphase flow
Microfluidics
Mixing
Liquid–liquid
Ionic liquids
PIV

ABSTRACT

Circulation patterns and mixing characteristics within water plugs in liquid/liquid segmented flow were investigated by means of micro-Particle Image Velocimetry. Experiments were carried out in a glass microchannel with circular cross-section of 100 μm radius using [C_4mim][NTf_2] ionic liquid as the carrier fluid. A T-junction was used as inlet, while mixture velocities varied from 0.0028 m/s to 0.0674 m/s. Two main circulation vortices were found within the plugs while at intermediate mixture velocities two additional secondary vortices appeared at the plug front. The mixing rate was locally quantified by means of the non-dimensional circulation time, which was calculated across the plug length. Consistently with the circulation patterns, the non-dimensional circulation time was found to have a profile along the direction of the flow that mirrors the shape of the plug, with a minimum at the axial location of the vortex cores (where the circulation velocity is maximum at the channel centre) while it tended to infinity towards the liquid/liquid interfaces. For all the experiments the minimum value of the circulation time fell within the range of 1.00–1.75. For increasing mixture velocities (i.e. increasing Ca) and sufficiently long plugs (ε_{IL}=0.4) a general decrease (i.e. higher mixing rate) of the circulation time minimum was found, although the behaviour was rather complex. On the other hand, the circulation velocity linearly increased as the *Ca* number (mixture velocity) increased.

1. Introduction

Two-phase microfluidic systems have been attracting increasing research interest for applications such as separations, mixing, encapsulation and chemical and biological analysis among others (Kreutzer et al., 2005; Wegmann and von Rohr, 2006; Kashid et al., 2007; Angeli and Gavriilidis, 2008; Ghaini et al., 2010; Jovanovic et al., 2011; Hardt and Hahn, 2012). Rapid and efficient mixing is a key feature in all these processes which may be particularly challenging in micro-units, due to the laminar nature of the flow at low Reynolds numbers. In many instances, the intensified mixing in a micro-device is a result of complex phenomena, which include micro-diffusion through thin fluid layers, recirculation patterns within phases, convection induced by surface tension gradients and flow instabilities between the two immiscible phases (Tung et al., 2009). One of the flow configurations that promotes mixing is plug or segmented flow (or Taylor flow for gas–liquid systems), where one phase flows within the other in the form of bubbles or drops (plugs) that have equivalent diameter larger than the channel diameter. Depending on the capillary number and the wall wetting characteristics there is usually a thin film separating the bubble/liquid plug from the channel wall (Angeli and Gavriilidis, 2008).

For understanding the mixing characteristics in two-phase microfluidic systems, details of the velocity profiles within the phases are required. Micro-Particle Image Velocimetry (μ-PIV) can be used to extract multipoint information of the velocity inside a single liquid plug or slug with high accuracy and spatial resolution and in a non-intrusive manner (Santiago et al., 1998; Lindken et al., 2009). Important mixing characteristics, such as the recirculation

* Correspondence to: Chemical Engineering Department, University College London, Torrington Place, London, WC1E 7JE, United Kingdom.
Tel.: +44 20 7679 3832; fax: +44 20 7383 2348.
E-mail address: p.angeli@ucl.ac.uk (P. Angeli).

0009-2509/$ - see front matter © 2012 Elsevier Ltd. All rights reserved.
http://dx.doi.org/10.1016/j.ces.2012.06.030

time, can then be derived from the velocity fields and other measured parameters, such as the location of stagnation points, vortex cores and plug/slug length. There have been a number of studies involving the application of μ-PIV on gas–liquid flows (Thulasidas et al., 1997; Günther et al., 2004; Waelchli and von Rohr, 2006; Van Steijn et al., 2007; Malsch et al., 2008), but only limited ones for liquid–liquid systems (Kashid et al., 2005; Sarrazin et al., 2006; Kinoshita et al., 2007; Wang et al., 2007; Fang et al., 2012). In these studies, μ-PIV has been used to visualize the internal recirculation in aqueous slugs or plugs during aqueous/oil two-phase flows. Kinoshita et al. (2007) obtained three-dimensional velocity information and circulation patterns inside a moving aqueous droplet by confocal microscopy, while other investigators (Kashid et al., 2005 and Sarrazin et al., 2006) qualitatively compared velocity fields acquired from PIV with CFD simulations, proving the suitability of the experimental technique for these flows. More recently, Fang et al. (2012) proposed a technique to locally enhance DNA concentration by using a plug flow micro-device. PIV velocity data within water plugs were used to locally quantify the shear strain rate, while mixing was investigated by using a continuous dye. Although previous investigations qualitatively related the velocity profiles from PIV to the mixing features, the latter was mainly quantified numerically or experimentally from dye dispersion. Local characterization of the mixing rate via parameters such as circulation time, important for mass transfer operations, is still missing in the literature for liquid–liquid plug flow configurations.

In this article, mixing patterns within water plugs in water/ionic liquid two-phase segmented flow in microfluidic channels have been investigated with μ-PIV and quantified via the non-dimensional circulation time. These studies are complementary to an ongoing research campaign on the use of ionic liquids for extraction applications in micro-separation units (Tsaoulidis et al., 2012). Ionic liquids are proposed here as green alternatives to organic solvents commonly used in extraction (Plechkova and Seddon, 2008). They are salts, liquid at room temperature, that have good thermal stability and very low vapour pressure, which ensure their use in a broad range of temperatures and minimize solvent losses. Most of them are also non-flammable and non-explosive, making them safer than organic solvents. Furthermore, their properties such as viscosity, density, polarity and solubility in water or other solvents can be tuned by an appropriate choice of anion and cation as well as chain length, allowing ionic liquids to be designed and optimized for a particular application (Binnemans, 2007). Despite their benefits, the industrial uptake of ionic liquids has been low mainly because of their high costs (Birdwell et al., 2006). Operation in intensified and microfluidic systems reduces the solvent volume required. The reduction in solvent volume is compensated by the high efficiencies achieved, because of the thin fluidic films formed in the confined spaces of the small channels, which can significantly reduce mass transfer resistances. Ionic liquids have already found numerous applications in processing (Binnemans, 2007; Plechkova and Seddon, 2008; Billard et al., 2011). Recently, they were applied to the enzymatic synthesis of isoamyl acetate in microchannels (Pohar et al., 2009), where yields much higher than in intensely mixed batch processes were found. Contrary to organic solvents however, ionic liquids have higher densities and viscosities than water which are expected to affect the two-phase hydrodynamics and mixing, as well as the flow pattern boundaries and pressure drop (Tsaoulidis et al., 2011). It was also found during preliminary experiments (not shown) that, despite their immiscibility with water, hydrophobic ionic liquids can exhibit wetting properties to materials such as glass and FEP similar to those of water, and result in more complex flow patterns that those obtained when organic solvents were used instead. These differences motivate new experimental investigations to characterize the hydrodynamics and mixing during segmented flow when ionic liquids are used as substitutes to organic solvents.

There are, to the authors knowledge, no previous μ-PIV studies on mixing in liquid–liquid microchannel flows, where one of the phases is an ionic liquid.

2. Circulation time

During plug (or segmented) liquid–liquid flow in small channels, as the liquid plug moves downstream the channel at constant speed, U_d, the fluid inside the plug circulates, forming counter rotating vortices with closed streamlines and a pattern symmetrical about the channel axis (Fig. 1). The rate of mixing inside the plug is then quantified through the circulation time. This is defined as the average time to displace material from one to the other end of the plug. The circulation time can then be normalized with the plug travel time, T, given by

$$T = \frac{U_d}{L_d} \tag{1}$$

where U_d is the plug speed and L_d is the plug length.

Assuming a fully developed laminar profile within the plug and the 3D flow model in Fig. 1, the non-dimensional circulation time in cylindrical coordinates (r,x), τ, reads as (Thulasidas et al., 1997)

$$\tau(x) = \frac{V}{Q}\frac{U_d}{L_d} = \frac{\pi L_d r_0^2/2}{\iint_{A_0} v(x,y,z)\,dA}\frac{U_d}{L_d} = \frac{U_d r_0^2}{2\int_0^{r_0} v(r,x)\,dr} \cong \frac{U_d r_0^2}{2\Delta r \sum_{i=1}^{i=N} v_i r_i|_x} \tag{2}$$

where V is the fluid volume, Q is the flow rate, r_0 is the location of the stagnation surface and v is the velocity.

When a planar domain at the centre of the channel is considered (i.e. π-plane in Fig. 1) and given the axisymmetric assumption, Eq. (2) is still valid when r is simply substituted with y. Alternatively, a two-dimensional definition of the non-dimensional circulation time can be obtained by rewriting Eq. (2), valid in a observation xy-plane π (Fig. 1)

$$\tau(x) = \frac{L_d y_0}{\int_0^{y_0} v(x,y)\,dy}\frac{U_d}{L_d} \cong \frac{U_d y_0}{\Delta y \sum_{i=1}^{i=N} v_i|_x} \tag{3}$$

where y_0 is the location of the stagnation point projected onto the observation mid-plane π (Fig. 1).

Eqs. (2) and (3) demonstrate how the measurement of local velocities and the knowledge of the structure of the internal recirculation (i.e. location of stagnation points) are essential for quantifying mixing inside the plug. Optical techniques such as μ-PIV are thus ideal to reconstruct the recirculation with high degree of detail.

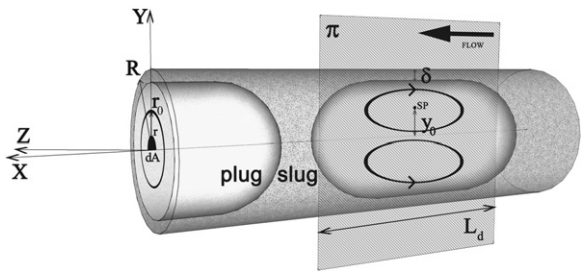

Fig. 1. Schematic of the flow pattern inside the microchannel of radius R in 3D (Eq. 2) and 2D (Eq. 3) reference frames. The internal recirculation parameters are sketched inside a single water plug, projected onto the mid-XY plane (π), where quantities in Eq. (3) are defined.

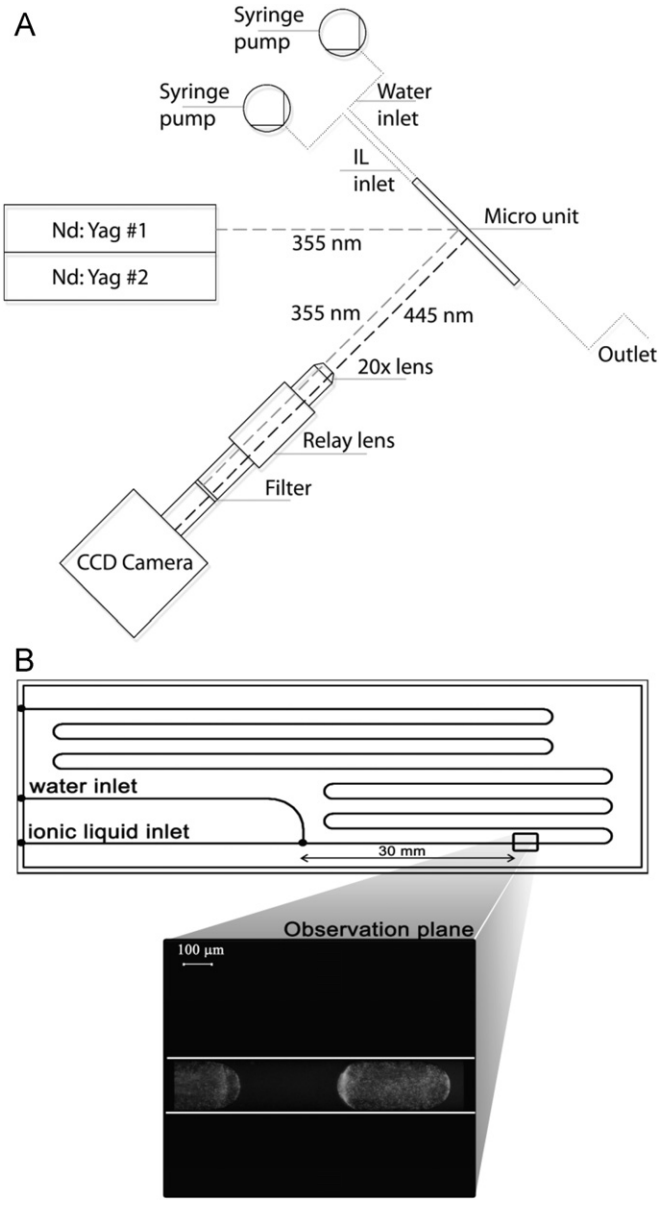

Fig. 2. Sketch of the experimental apparatus (A). Side view of the microchannel (B). Cross-section is circular with radius of 100 μm. The observation plane (*XY*) is positioned downstream about 30 mm away from the T-inlet. Drawing not to scale.

3. Experimental apparatus and procedures

The experimental setup is sketched in Fig. 2A. Tests were carried out in a quartz microchannel with circular cross-section of radius, R, of 100 μm (Fig. 2B). The channel was etched in a quartz chip, which was sealed through thermal bonding (Dolomite microfluidics). Deionised water and $[C_4mim][NTf_2]$ ionic liquid, of density of 1420 kg/m^3, viscosity of 0.029 Pa s and surface tension of 0.032 N/m, were employed as working fluids. The two liquid phases were brought together co-currently in a T-shaped inlet, which was also etched on the chip and whose branches were of the same size as the main channel. Two syringe pumps (KDS scientific) dispensed the working fluids inside the test channels at constant flow rates. Flexible Teflon tubing (Upchurch 1/16 in. OD FEP tubing) was used to connect the outlets of the pumps with the T-inlet. Experiments were carried out at different combinations of mixture velocities based on input phase flow rates ($U_{mix}=[Q_w+Q_{IL}]/[\pi R^2]$, where Q_w and Q_{IL} are the water and ionic liquid input flow rates, respectively) and ionic liquid volume fractions ($\varepsilon_{IL}=Q_{IL}/[Q_w+Q_{IL}]$) as shown in Table 1. For all the experiments the aqueous phase was seeded with 1 μm polymer micro-beads suspension at 0.1% concentration by weight. These seeding particles are internally dyed with a blue fluorophore (Thermo Scientific 365/445 nm).

A UV double pulsed Nd:YAG laser (TSI instruments) illuminated the microfluidic device from a 45° angle with a 355 nm beam (volume illumination). The observation region was 30 mm away from the inlet. The laser beams excited the particles which emitted blue light within a band centred on 445 nm. Particle blue fluorescence was detected by a 12-bit 4 Mpixels 16 fps CCD camera (TSI instruments), focused on the test section, after passing through a narrow pass band filter centred at 445 nm. The optical train (TSI instruments) mounted on the camera allowed 20 × magnification, flat-field and aberration correction to be achieved. The used optical system provided a field of view of the order of 1 mm and a pixel size projected back onto the flow of 0.53 μm. The focal plane was located at the centre of the channel along the z direction (the focal plane was located with a precision traverse, which had been pre-calibrated using the front wall as a reference and maximizing the channel width, giving an uncertainty of ± 1 μm). According to the numerical aperture of the magnification lens (NA=0.42 and $n=1.00$) and features of seeding particles the depth of field was of the order of 3 μm and the depth of correlation (2 z_{corr}, i.e. resolution along the z direction) for PIV measurements was about 8 μm (Olsen and Adrian, 2000). The refractive index of the ionic liquid (i.e. 1.51, Deetlefs et al., 2006) matched well that of the channel material (i.e. 1.54) and refraction at the inner channel wall/liquid interface can be neglected, as the ionic liquid in all studied cases was in contact with the channel wall. In addition, the external channel wall was flat and it was not necessary to add a third medium for refractive index matching (Budwig, 1994; Han and Shikazono 2009). Furthermore, typical distortion/reflection effects due to refraction at solid/liquid and liquid/liquid interfaces as described by Budwig (1994) were not observable on the acquired images.

Images were acquired in straddle mode by a frame grabber and stored in the hard disk of a PC. The image acquisition was synchronized with laser pulses in such a way that image pairs were captured at a maximum frequency of 7 Hz, while the time lag between the two images of a pair (i.e. dt, the time lag between two laser pulses) was adjusted according to the expected velocity inside the channel and the required spatial resolution. For the present experiments, dt was varied between 20 and 1000 μs, depending on the combination of flow rates inside the channel.

In order to measure velocity components inside a regular grid drawn on the measurement plane, the domain in each image was sampled into rectangular-shaped interrogation windows properly overlapped to satisfy the Nyquist sampling criterion (Meinhart et al., 1999). A standard PIV algorithm (TSI instruments) was used to reconstruct the displacement of each window across the two images of a pair via a cross-correlation routine with sub-pixel accuracy. The two-component velocity field could thus be reconstructed within the Eulerian grid in which the domain had been discretized, by employing the spatial calibration ratio and the time lag between the correlation images. In the present experiments a square domain discretization of 32 × 32 pixels with 50% overlap was implemented that provided robust statistics and a velocity spatial resolution of 8.48 μm. By properly adjusting the time lag, the maximum displacement between the two images of a pair never exceeded 25% of the window size. This criterion minimizes the effect of the error increase on velocity measurements as the maximum displacement increases. The uncertainty of the velocity measurements can be estimated from the diffraction limited theory (Meinhart et al., 1999). The effective particle diameter projected back onto the flow, d_{eff}, given by the

Table 1
Overview of runs at varying ionic liquid flow rates (Q_{IL}) and input volume fractions (ε_{IL}). Average and standard deviation values (std) were calculated over 8 s (60 samples).

Input parameters					$L_d \times 10^{-3}$ (m)	std_{Ld} (%)	$\delta \times 10^{-6}$ (m)	std_δ (%)	U_d (m/s)	τ_{min}
Exp.	ε_{IL} $Q_{IL}/[Q_w+Q_{IL}]$	Q_{IL} (ml/h)	U_{mix} (m/s)	Ca $\frac{\mu_{IL}U_{mix}}{\sigma}$						
1	0.6	0.2	0.0028	0.007	0.3290	4.8	14.7	4.7	0.0030	1.59
2	0.5	0.2	0.0037	0.009	0.4304	5.7	13.8	5.0	0.0031	1.43
3	0.4	0.2	0.0042	0.010	0.5512	0.9	14.3	4.8	0.0046	1.43
4	0.6	0.4	0.0056	0.013	0.3461	1.0	17.7	6.7	0.0051	1.75
5	0.5	0.4	0.0067	0.016	0.4361	0.9	17.0	5.2	0.0064	1.43
6	0.4	0.4	0.0084	0.020	0.5459	0.9	17.8	4.4	0.0084	1.43
7	0.6	0.8	0.0112	0.026	0.3832	3.9	19.0	5.7	0.0082	1.63
8	0.5	0.8	0.0135	0.032	0.3841	1.2	19.1	0.5	0.0122	1.21
9	0.4	0.8	0.0169	0.040	0.5270	1.1	21.0	0.4	0.0196	1.45
10	0.6	1.6	0.0225	0.053	0.3188	1.2	23.0	5.6	0.0239	1.19
11	0.5	1.6	0.0270	0.064	0.3840	1.3	24.0	3.7	0.0255	1.42
12	0.4	1.6	0.0337	0.080	0.4554	0.9	25.6	3.5	0.0376	1.14
13	0.6	3.2	0.0449	0.106	0.26010	1.3	27.4	4.7	0.05461	1.47
14	0.5	3.2	0.0539	0.127	0.31665	1.1	29.6	3.7	0.07891	1.34
15	0.4	3.2	0.0674	0.159	0.40479	1.8	31.7	3.1	0.07567	1.00

diffraction limited point spread function d_s was calculated to be 1.6 μm (3–4 pixels). This allows a location of the particle image correlation peak to be determined within one-tenth of the particle image diameter, d_{eff}, which results in a displacement uncertainty of 0.16 μm in this case. For the minimum time lag employed in the present investigation (i.e. 20 μs) at corresponding average velocity of 0.067 m/s, the uncertainty is found to be of the order of 0.01%.

The flow under investigation can be considered steady state with respect to a reference frame attached to the moving plug, in which case ensemble averaging is possible. Given the intermittent nature of the flow, an in-house pre-processing routine was developed to identify the moving water plug over the image sequence and translate it to the same reference frame. The same pre-processing routine was also employed to measure key features such as channel diameter (D), plug length (L_d), and width (W_d) with a pixel accuracy (± 0.27 μm) by image thresholding and binarization. The ionic liquid film thickness was then derived by using the following relation:

$$\delta = \frac{D - W_d}{2} \tag{4}$$

4. Results and discussion

An overview of the experimental runs is given in Table 1, where experimental conditions and key parameters measured using PIV are reported. For all experimental conditions, water formed the plug phase and ionic liquid the carrier continuous phase.

4.1. Plug length and film thickness

The plug length, L_d, and the film thickness, δ, were measured by analyzing the images acquired using the PIV setup. The plug interfaces were easily detected with an edge detection routine on binary images obtained using the pre-processing routine described in Section 3. The values were averaged over a set of 60 images while the error was estimated by the standard deviation of the sample (std_{Ld} and std_δ in Table 1). It was found that very regular plug length and film thickness were established inside the microchannel as indicated by the low values of the standard deviation (about 2% and 4% on average, respectively).

In Fig. 3 the dimensionless water plug length (L_d/R) is plotted as a function of the capillary number for 3 different ionic liquid input volume fractions ε_{IL} (0.6, 0.5 and 0.4). The capillary number, Ca, is defined below as a function of ionic liquid viscosity, μ_{IL}, mixture velocity, U_{mix}, and interfacial tension between water and ionic liquid, σ (12.29 mN/m):

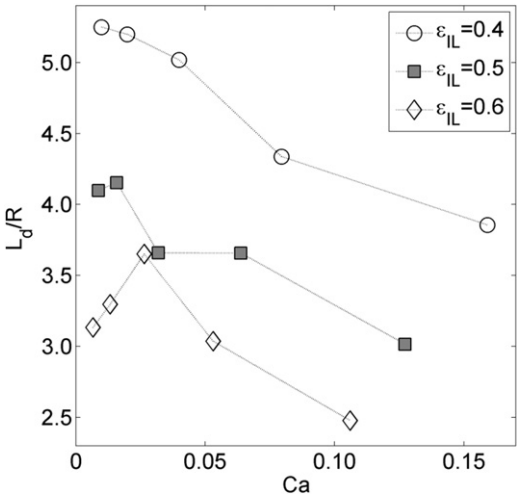

Fig. 3. Non-dimensional water plug length as a function Ca number for three volume fractions of the carrier fluid. L_d is the average plug length and R is the channel radius.

$$Ca = \frac{\mu_{IL} U_{mix}}{\sigma} \tag{5}$$

At low velocities the plug length slightly varies as Ca (i.e. mixture velocity) increases and tends to decrease as Ca increases further. For the whole range of mixture velocities, the plug length consistently decreases as the volume fraction of the carrier ionic liquid increases.

The film thickness is found to be mainly a function of the mixture velocity (i.e. capillary number, Ca) and tends to increases as the velocity increases. In Fig. 4 the non-dimensional film thickness (δ/R) found using Eq. (4) is plotted as a function of Ca. Experimental results are compared with Taylor (1961) and Bretherton (1961), eq. (6), Irandoust and Anderson (1989), eq. (7), and Aussillous and Quéré (2000), eq. (8), models. The model by Irandoust and Anderson, eq. (7), is the closest to the present results.

$$\frac{\delta}{R} = 0.5\, Ca^{1/2} \tag{6}$$

$$\frac{\delta}{R} = 0.36\left[1 - \exp(-3.08\, Ca^{0.54})\right] \tag{7}$$

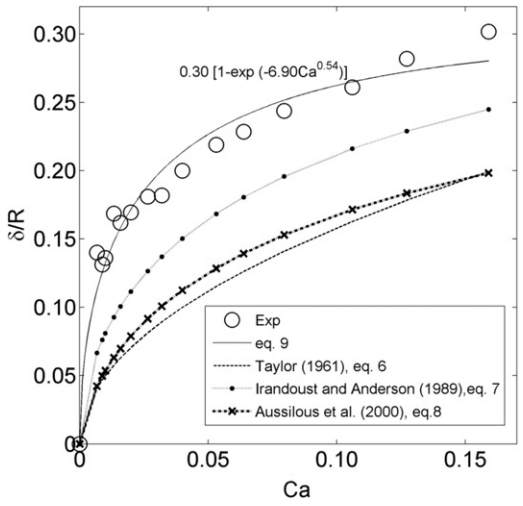

Fig. 4. Non-dimensional film thickness as a function of *Ca* number. δ is the average film thickness and *R* is the channel radius. Comparisons with the literature models are superimposed on the present experimental results.

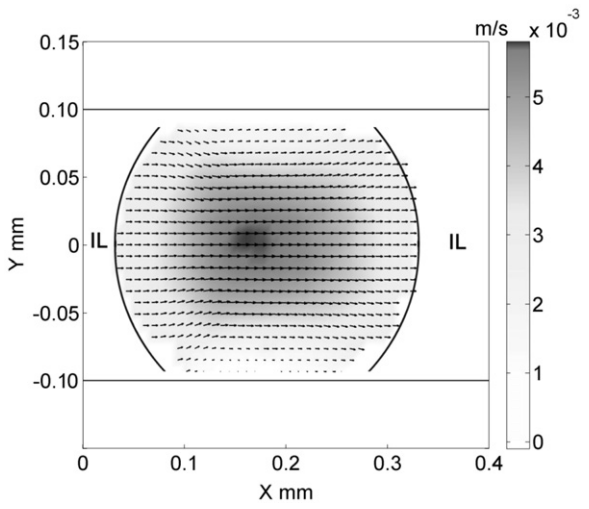

Fig. 5. Ensemble averaged velocity field for exp#1. The magnitude of the velocity is superimposed in grey scale colours.

$$\frac{\delta}{R}=\frac{1.34\,Ca^{2/3}}{1+2.5(1.34\,Ca^{2/3})} \tag{8}$$

A best fit curve was also found, Eq. (9), which resembles the model of Irandoust and Anderson (1989)

$$\frac{\delta}{R}=0.30\left[1-\exp(-6.90\,Ca^{0.54})\right] \tag{9}$$

It is worth noting here that, to the best of our knowledge, there are no experimental correlations for the film thickness in the literature for the fluidic system employed in this study. The correlations available are for gas/liquid systems, which provide thinner δ/R than the present results ($0.138<\delta/R<0.317$, for $0.0028\ \text{m/s}<U_{mix}<0.0674\ \text{m/s}$) (Fig. 4). Ghaini et al. (2011) also found experimentally a thinner δ/R (i.e. $\delta/R=0.015$ at around 0.07 m/s slug velocity) for a water/kerosene fluidic system in a glass capillary with 1 mm ID. The large film thickness values in the present work may be due to the higher *Ca* number achieved at relatively low mixture velocities because of the high viscosity of the ionic liquid. Commonly in the literature high *Ca* numbers are obtained by increasing mixture velocity rather than fluid viscosity.

4.2. Plug speed

Fig. 5 shows a sample total velocity field, within a single water plug, ensemble averaged over more than 60 cross-correlated image pairs (reference frame is stationary and attached to the image). It can clearly be seen that the horizontal component of the velocity is dominant as the main flow direction is along the *x*-axis. The magnitude of the velocity is maximum at the core of the plug, while it is decreasing towards the channel walls and the liquid/liquid interfaces. Since the plug is moving at constant speed U_d, the internal recirculation is not apparent if a stationary reference frame is employed as in Fig. 5. By subtracting U_d from the total velocity field (i.e. reference frame attached to the moving plug), the internal recirculation is revealed. Therefore, the plug speed U_d needs to be found experimentally from the profiles of the streamwise component of velocity along the direction of the flow.

Sample profiles of the horizontal component of the velocity along the plug are shown in Fig. 6 for the same experiment presented in Fig. 5. For all the experiments, a laminar profile is fully established at the centre of the plug. The velocity decreases

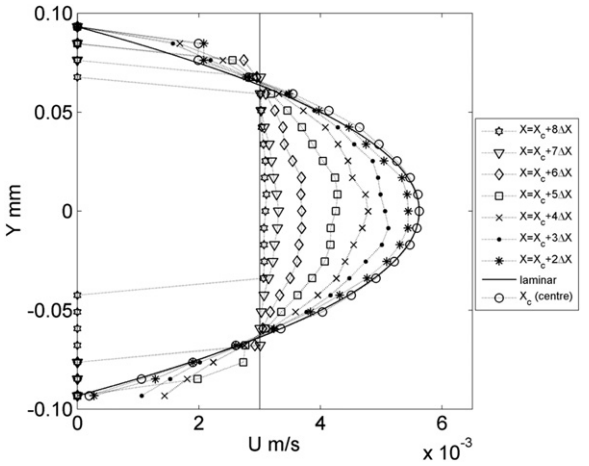

Fig. 6. Vertical profiles of the horizontal component of the total velocity across half of the water plug for exp#1. X_c is the axial location of the plug centre, while the spacing between profiles, Δ, is approximately equal to 24 μm.

and the profiles become more uniform as the interface is approached. The profiles are symmetrical about the channel axis. The average plug speed, U_d, is defined here as the value of the velocity where all the profiles intersect, which coincides with the average velocity at the liquid/liquid interfaces. The value found experimentally is very close to the mixture velocity as shown in Table 1.

4.3. Circulation patterns

The circulation patterns inside the plugs were obtained by subtracting the plug speed U_d from the total velocity vector field measured using PIV. Three different regimes are found depending on the mixture velocity as shown in Fig. 7. For relatively low mixture velocities (0.0028–0.0042 m/s), the circulation pattern consists of two distinct vortices, counter rotating and symmetrical about the channel axis. Two stagnation points at the vortex cores are clearly visible, which move towards the rear of the plug when the plug length decreases (i.e. the ionic liquid volume fraction increases). On the contrary, larger plugs exhibit a more symmetrical circulation pattern with respect to the plug centreline.

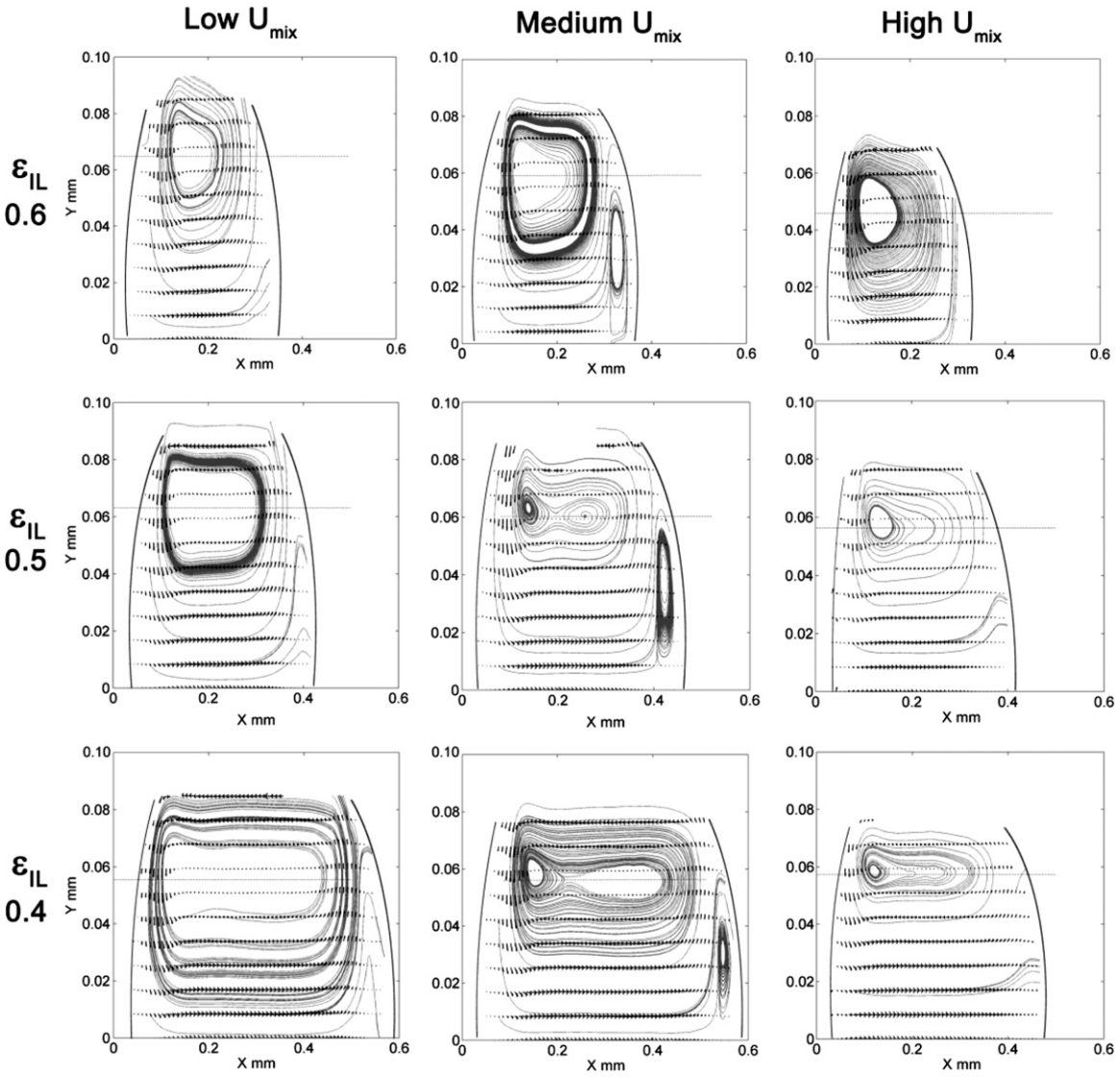

Fig. 7. Representative circulation patterns in the top half of water plugs found for the three regimes depending on mixture velocity, as a function of input ionic liquid volume fraction.

For intermediate mixture velocities (0.0056–0.0169 m/s), two extra vortices appear at the front of the plugs, which for small plugs, occupy a significant area. As a result of the higher speed of the carrier fluid the rear interface is more flat compared to the lower velocity, while the front interface is sharper, exhibiting a "bullet" shape. The fluid can thus recirculate also within the sharp nose. The stagnation points move towards the rear of the plug as the volume fraction increases (plug size decreases), similar to what was seen at lower mixture velocities.

For relatively high mixture velocities (0.0225–0.0674 m/s), the plugs again exhibit the two counter rotating vortices and a smoother plug shape (i.e. contact angles at the rear and front interfaces are close). However, as a result of a thicker film at the channel walls the plug seems "squeezed" against the channel axis and the stagnation points slightly move towards the channel centreline.

4.4. Circulation time

A sample of the non-dimensional circulation time profile across the length of the water plug is shown in Fig. 8c, which was calculated using Eq. (3) with the 2D PIV circulation velocity data (Table 1). If Eq. (2) is used instead, the circulation time is averaged over the cross-sectional area (3D model) and a slightly larger circulation time is found (not shown). This result is consistent with the fact that the velocity averaged along the *y*-direction within the *XY* mid-plane is expected to be higher than the average velocity within the whole channel depth, thus giving rise to smaller circulation time. For all the experiments, the circulation time reaches a minimum value at the axial location of the vortex cores, where the average velocity is maximum as the comparison between the circulation velocity field (Fig. 8a) and the velocity magnitude map (Fig. 8b) demonstrates. Towards the water/ionic liquid interfaces the circulation time tends to infinity, as it cannot be defined where the laminar profile is not developed. The minimum value of τ falls within the range of 1.00–1.75. It is worth noting here that previous studies on Taylor flow (Thulasidas et al., 1997) used Eq. (2) to calculate the non-dimensional circulation time, which always gives slightly larger values. In addition, previous investigators did not consider the variation of the circulation time along the length of the plug and computed it at the centre of the plug only. This implied the assumption of symmetry about both the plug axes and a laminar profile at the centre of the plug. In the liquid–liquid system under investigation though, an asymmetry about the plug centreline is

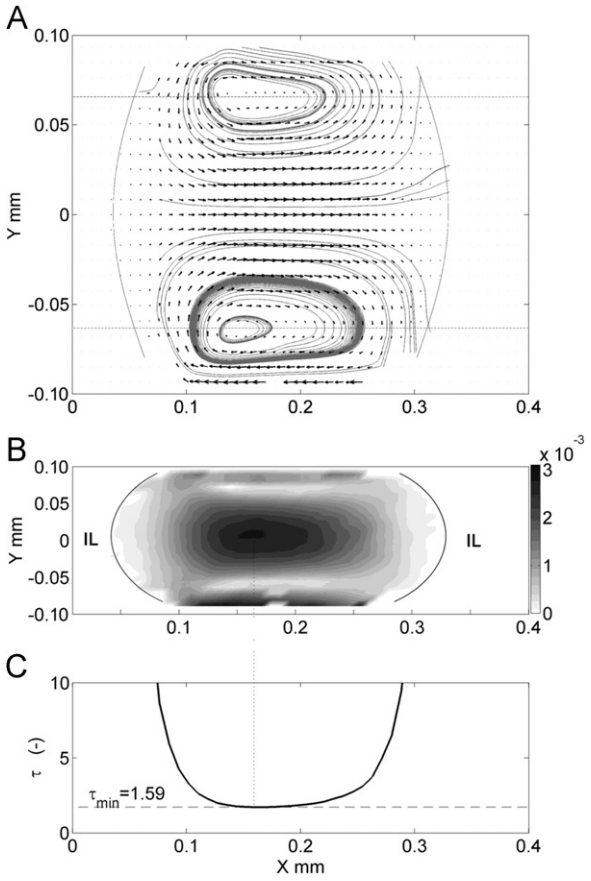

Fig. 8. Circulation pattern (*A*), magnitude of circulation velocity in grey scale (*B*) and non-dimensional circulation time (τ) profile (C) for exp#1, calculated using Eq. (3). The minimum of τ is at the axial location of the vortex cores (i.e. maximum of circulation velocity at the channel centreline).

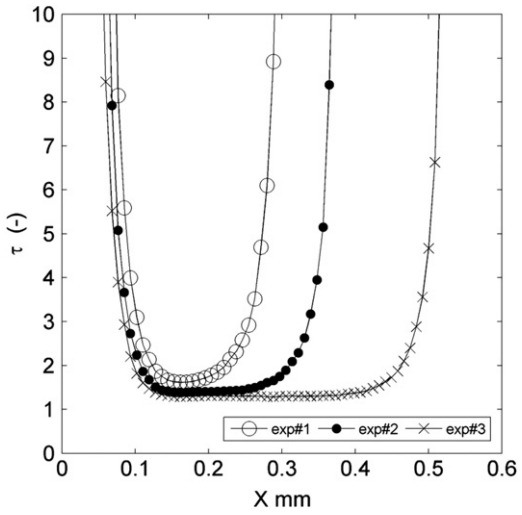

Fig. 9. Non-dimensional circulation time profiles across the water plug for different input ionic liquid volume fraction at low mixture velocities.

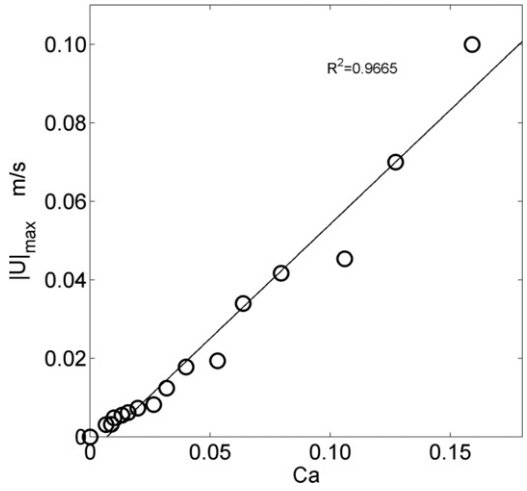

Fig. 10. Maximum circulation velocity at the centre of the plug as a function of the *Ca* number.

generally observed, which is larger for shorter plugs (i.e. higher ε_{IL}, Fig. 7). Only in the case of large plugs the PIV results demonstrate a fair symmetry of the circulation patterns.

Circulation time along the plug can be seen in Fig. 9 for plugs of different lengths (different ε_{IL}). The circulation time, and the mixing rate, are fairly constant across the length of large plugs where circulation patterns are symmetric. On the contrary, for shorter plugs, since the vortex cores are pushed towards the rear interface (Figs. 7 and 8), the circulation patterns are not symmetric and the minimum of the circulation time is shifted along the *x*-axis towards the vortex cores. Moreover, the locations of the stagnation points along the *y*-direction (lines of zero circulation velocity in Fig. 8a and b) are influenced by the ionic liquid film thickness at the wall, which thus plays an important role in the mixing rate.

The variation of the maximum of the circulation velocity with the *Ca* number is depicted in Fig. 10. For all the ε_{IL}, as the mixture velocity increases (i.e. *Ca* number increases) the circulation velocity increases almost linearly. The film thickness also increases consistently as shown in Fig. 4, resulting in a smaller y_0, the vertical location of the stagnation point. Therefore, the circulation time tends to decrease as the mixture velocity is increased, providing a higher mixing rate. This can be seen in Fig. 11 where the minimum circulation time is plotted against the *Ca* number. However, while the circulation velocity clearly correlates with the mixture velocity through a fairly linear trend (Fig. 10), a straightforward correlation with the mixture velocity is not established for the circulation time (Fig. 11). This suggests that the circulation time, and thus the mixing rate, is a more complex function of other hydrodynamic parameters including not only circulation velocity but also location of the stagnation points and the film thickness, which in turn influences the vertical location of the stagnation points. This lack of a clear correlation in Fig. 11 is particularly true for shorter plugs and intermediate velocities, where the circulation patterns show anomalies (see Fig. 7). On the other hand, for relatively long plugs (ε_{IL}=0.4), the decreasing trend of the minimum of circulation time with *Ca* (Fig. 11) is well consistent with the increasing trend of the maximum of circulation velocity (Fig. 10), providing optimal conditions for the mixing rate.

5. Conclusions

The local hydrodynamics and the circulation time during water/ionic liquid segmented flow in a circular glass microchannel are determined within a water plug using μ-PIV. Mixing characteristics inside a single water plug are derived in a reference system attached to the moving plug. At low and high mixture velocities two vortices are formed within the water plug, symmetric about the channel axis. At intermediate velocities the

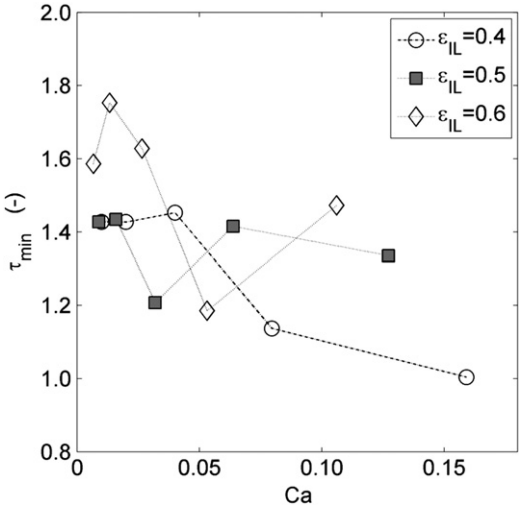

Fig. 11. Minimum of non-dimensional circulation time as a function of *Ca* number and for varying input ionic liquid volume fraction.

plug acquires a bullet shape and two secondary small vortices appear close to the plug nose.

Consistently with the circulation patterns, a minimum value of circulation time τ ($1.00 < \tau_{min} < 1.75$) is found at the axial location of the vortex cores, which are pushed toward the rear interface for shorter plugs. On the other hand, longer plugs show a more uniform τ along the axial direction. The maximum circulation velocity is found to increase almost linearly with increasing *Ca*. For sufficiently long plugs ($\varepsilon_{IL}=0.4$), the minimum circulation time, τ_{min}, tends to decrease as the *Ca* number increases, in accordance with the maximum of circulation velocity. However, the behaviour of τ_{min} as a function of Ca is more complex for shorter plugs and intermediate velocities, where anomalies in the circulation pattern were found.

In future work the mixing patterns and circulation time will be related to the mass transfer characteristics of the ionic liquid–water plug flow system.

Acknowledgements

The authors are grateful to the UK Engineering and Physical Sciences Research Council (EPSRC) and the UCL Energy Institute for funding the project. Special acknowledgements go to Prof. Kenneth R. Seddon and Dr. Natalia Plechkova of Queen's University Ionic Liquid Laboratories (QUILL) for providing the ionic liquid.

References

Angeli, P., Gavriilidis, A., 2008. Hydrodynamics of Taylor flow in small channels: a review. Proc. Inst. Mech. Eng. C—J. Mech. Eng. Sci. 222 (5), 737–751.

Aussillous, P., Quéré, D., 2000. Quick deposition of a fluid on the wall of a tube. Phys. Fluids 12 (10), 2367–2371.

Billard, I., Quadi, A., Jobin, E., Champion, J., Gaillard, C., Georg, S., 2011. Understanding the extraction mechanism in ionic liquids: UO2+/HNO3/TBP/C4-mimTf2N as a case study. Solvent Extr. Ion Exch. 29, 577–601.

Binnemans, K., 2007. Lanthanides and actinides in ionic liquids. Chem. Rev. 107, 2592–2614.

Birdwell, J.F., McFarlane, J., Hunt, R.D., Luo, H., DePaoli, D.W., 2006. Separation of ionic liquid dispersions in centrifugal solvent extraction contactors. Sep. Sci. Technol. 41, 2205–2223.

Bretherton, F.P., 1961. The motion of Long bubbles in tubes. J. Fluid Mech. 10, 166–188.

Budwig, R., 1994. Refractive index matching methods for liquid flow investigations. Exp. Fluids 17, 350–355.

Deetlefs, M., Seddon, K.R., Shara, M., 2006. Predicting physical properties of ionic liquids. Phys. Chem. Chem. Phys. 8, 642–649.

Fang, W.F., Ting, S.C., Hsu, C.W., Chen, Y.T., Yang, J.T., 2012. Locally enhanced concentration and detection of oligonucleotides in a plug-based microfluidic device. Lab Chip 12, 923–931.

Ghaini, A., Kashid, M.N., Agar, D.W, 2010. Effective interfacial area for mass transfer in the liquid–liquid slug flow capillary microreactors. Chem. Eng. Process. 49 (4), 358–366.

Ghaini, A., Mescher, A., Agar, D.W., 2011. Hydrodynamic studies of liquid–liquid slug flows in circular microchannels. Chem. Eng. Sci. 66, 1168–1178.

Günther, A., Khan, S.A., Thalmann, M., Trachsel, F., Jensen, K.F., 2004. Transport and reaction in microscale segmented gas–liquid flow. Lab Chip 4, 278–286.

Han, Y., Shikazono, N., 2009. Measurement of the liquid film thickness in micro tube slug flow. Int. J. Heat Fluid Flow 30, 842–853.

Hardt, S., Hahn, T., 2012. Microfluidics with acqueous two-phase systems. Lab Chip 12, 434–442.

Irandoust, S., Anderson, B., 1989. Liquid film in Taylor flow through a capillary. Ind. Eng. Chem 28, 1684–1688.

Jovanovic, J., Zhou, W., Rebrov, E.V., Nijhuis, T.A., Hessel, V., Schouten, J.C., 2011. Liquid–liquid slug flow: hydrodynamics and pressure drop. Chem. Eng. Sci. 66, 42–54.

Kashid, M.N., Gerlach, I., Goetz, S., Franzke, J., Acker, J.F., Platte, F., Agar, D.W., Turek, S., 2005. Internal circulation within the liquid slugs of a liquid−liquid slug-flow capillary microreactor. Ind. Eng. Chem. Res. 44 (14), 5003–5010.

Kashid, M.N., Madhvanand, N., Agar, D.W., 2007. Hydrodynamics of liquid–liquid slug flow capillary microreactor: flow regimes, slug size and pressure drop. Chem. Eng. J. 131, 1–13.

Kinoshita, H., Kaneda, S., Fujii, T., Oshima, M., 2007. Three-dimensional measurement and visualization of internal flow of a moving droplet using confocal micro-PIV. Lab Chip 7 (3), 338–346.

Kreutzer, M.T., Kapteijn, F., Moulijin, J.A., Heiszwolf, J.J., 2005. Multiphase monolith reactors: chemical reaction engineering of segmented flow in microchannels. Chem. Eng. Sci. 60, 5895–5916.

Lindken, R., Rossi, M., Große, S., Westerweel, J., 2009. Micro-particle image velocimetry (microPIV): recent developments, applications, and guidelines. Lab Chip 9 (17), 2551–2567.

Malsch, D., Kielpinski, M., Merthan, R., Albert, J., Mayer, G., Köhler, J.M., Süße, H., Stahl, M., Henkel, T., 2008. μPIV-analysis of Taylor flow in micro channels. Chem. Eng. J. 135 (1), S166–S172, no. 0.

Meinhart, C.D., Werely, S.T., Santiago, J.G., 1999. PIV measurements of a microchannel flow. Exp. Fluids 27, 414–419.

Olsen, M.G., Adrian, R.J., 2000. Out-of-focus effects on particle image visibility and correlation in microscopic particle image velocimetry. Exp. Fluid, S166–S174 (Suppl.).

Plechkova, N., Seddon, K.R., 2008. Applications of ionic liquids in the chemical industry. Chem. Soc. Rev. 37, 123–150.

Pohar, A., Plazl, I., Znidarsic-Plazl, P., 2009. Lipase-catalyzed synthesis of isoamyl acetate in an ionic liquid/*n*-heptane two-phase system at the microreactor scale. Lab Chip 9 (23), 3385–3390.

Santiago, J.G., Wereley, S.T., Meinhart, C.D., Beebe, D.J., Adrian, R.J., 1998. A particle image velocimetry system for microfluidics. Exp. Fluid 25, 316–319.

Sarrazin, F., Loubière, K., Prat, L., Gourdon, C., Bonometti, T., Magnaudet, J., 2006. Experimental and numerical study of droplets hydrodynamics in microchannels. AIChE J. 52 (12), 4061–4070.

Taylor, G.I., 1961. Deposition of a viscous fluid on the wall of a tube. J. Fluid Mech. 10, 161–165.

Thulasidas, T.C., Abraham, M.A., Cerro, R.L., 1997. Flow patterns in liquid slugs during bubble-train flow inside capillaries. Chem. Eng. Sci. 52 (17), 2947–2962.

Tsaoulidis D., Dore V., Angeli P., Plechkova N.V., and Seddon K.R., 2011. Liquid–liquid flows in microchannels. In: Proceedings of the Third Micro and Nano Flows Conference, 22–24 August, Thessaloniki, Greece.

Tsaoulidis, D., Dore, V., and Angeli, P., 2012. Microchannel extractions using ionic liquids for spent nuclear fuel reprocessing. In: Proceedings of International Conference on Microreaction Technoology, 20th–22nd February 2012, Lyon, France.

Tung, K.Y., Li, C.C., Yang, J.T., 2009. Mixing and hydrodynamic analysis of a droplet in a planar serpentine micromixer. Microfluid. Nanofluid. 7 (4), 545–557.

Van Steijn, V., Kreutzer, M.T., Kleijn, C.R., 2007. μ-Piv study of the formation of segmented flow in microfluidic T-junctions. Chem. Eng. Sci. 62 (24), 7505–7514.

Waelchli, S., von Rohr, P.R., 2006. Two-phase flow characteristics in gas–liquid microreactors. Int. J. Multiphase Flow 32 (7), 791–806.

Wang, C., Nguyen, N.-T., Wong, T.N., 2007. Optical measurement of flow field and concentration field inside a moving nanoliter droplet. Sens. Actuat. A: Phys. 133 (2), 317–322.

Wegmann, A., von Rohr, P.R., 2006. Two phase liquid–liquid flows in pipes of small diameters. Int. J. Multiphase Flow 32 (8), 1017–1028.